J. exp. Biol. (1976), 65, 577–602
With 8 figures
Printed in Great Britain

SPIRILLUM SWIMMING: THEORY AND OBSERVATIONS OF PROPULSION BY THE FLAGELLAR BUNDLE

BY H. WINET AND S. R. KELLER*

California Institute of Technology,
Division of Engineering and Applied Science, Pasadena, California 91125

(*Received* 4 *June* 1976)

SUMMARY

The hydrodynamics and energetics of helical swimming by the bacterium *Spirillum* sp. is analysed using observations from medium speed cine photomicrography and theory. The photographic records show that the swimming organism's flagellar bundles beat in a helical fashion just as other bacterial flagella do. The data are analysed according to the rotational resistive theory of Chwang & Wu (1971) in a simple-to-use parametric form with the viscous coefficients C_s and C_n calculated according to the method of Lighthill (1975). Results of the analysis show that *Spirillum* dissipates biochemical energy in performing work against fluid resistance to motion at an average rate of about 6×10^{-8} dyne cm s^{-1} with some 62–72 % of the power dissipation due to the non-contractile body. These relationships yield a relatively low hydromechanical efficiency which is reflected in swimming speeds much smaller than a representative eukaryote. In addition the C_n/C_s ratio for the body is shown to lie in the range 0·86–1·51 and that for the flagellar bundle in the range 1·46–1·63. The implications of the power calculations for the Berg & Anderson (1973) rotating shaft model are discussed and it is shown that a rotational resistive theory analysis predicts a 5-cross bridge M ring for each flagellum of *Spirillum*.

INTRODUCTION

All flagellated micro-organisms must divide the biochemical energy they generate into the performance of biosynthetic, molecular transport and mechanical work. The relative rates at which this energy is dissipated (the power) in the various work functions is one measure of the relative survival value of the function in question. Absolute values for power cost can provide the limits within which models for the processes by which each of the three kinds of work is carried out must remain. Moreover, since energy relationships are common denominators for all cell activities, they can be used to trace the causal connexions between the three work processes.

The procedures described in this report can be used to calculate the power cost to any flagellated micro-organism of overcoming fluid resistance to propulsion. The present case is particularly illustrative because the geometry of the flagellar beat is not readily apparent, so a variety of possibilities are explored. The fact that the organism is a

* Present address: Department of Civil Engineering and Engineering Mechanics, Columbia University, New York, N.Y. 10027.

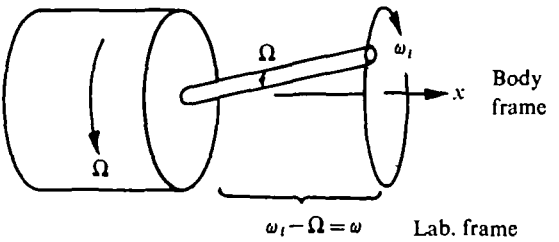

Fig. 1. The balancing of angular momentum which extends the resistive theory of Gray & Hancock (1955) to the rotational resistive theory of Chwang & Wu (1971). The flagellum would rotate at angular velocity ω_t if the body were held fast. In the free fluid however, the body counter rotates – as must the bundle to keep from twisting off – until it attains a steady angular velocity Ω at which the total angular momentum is balanced.

prokaryote imposes no limits on the calculation of dynamic quantities – force, moment, etc. – but the values generated by this analysis are of prime importance to the development of a model for prokaryote flagellar oscillation.

Calculation of power requirements for mechanical work usually proceed from a determination of the forces and moments imposed on the system at work by the resisting environment. Where force is F and swimming velocity is U the power P is readily calculated as a form of $F.U$ in dyne cm s^{-1}. The energy dissipated over a period of time t a form of $P.t$ which is related to work by the first law of thermodynamics.

The organism of interest in the present analysis is the bacterium *Spirillum*. The fluid-mechanical model by which forces and moments are calculated is the rotational resistive theory developed by Chwang & Wu (1971). This theory for flagellum-propelled micro-organisms was developed for three-dimensional flagellar beats from the two-dimensional theory of Gray & Hancock (1955). Chwang, Wu & Winet (1972, hereafter to be designated CWW) have in fact, used measurements of Spirillum locomotion obtained by Metzner (1921) to calculate dynamic quantities for this organism. We shall show, however, that the flagellar beat geometry interpreted from Metzner's drawings – and consequently the resulting CWW model – are oversimplified. In the CWW model, as in all analyses based upon rotational resistive theory, a tail, flagellum, or, as is the case with Spirillum, a flagellar bundle tries to 'whip about' at some angular velocity ω_t, as indicated in Fig. 1. The fluid reacts to ω_t, in balancing the angular momentum, with a viscous resistance which has the effect of counter-rotating the non-flexible body and attached bundle at an angular velocity Ω. As a result of this balancing an observer sitting on the body sees the tail whipping about at ω_t but an observer in the fixed lab system sees an apparent tail rotation velocity of

$$\omega_t - \Omega = \omega. \tag{1}$$

In order to produce forward motion, the body and/or bundle must propagate a travelling wave which can push the fluid continuously, generating a viscous fluid reaction in the direction of the rotation axis which we shall term the x axis. In the case of Spirillum the rigid body is already helical in shape so it can generate an x fluid force component in reaction to the rigid wave whose balance propagation velocity is $\Omega/k_b = c_b$ where $k_b = 2\pi/\lambda_b$ the wave constant, with λ_b the rigid helix wavelength. When the fluid forces generated by c_b and the moments of force (or torques) generated by ω and Ω are

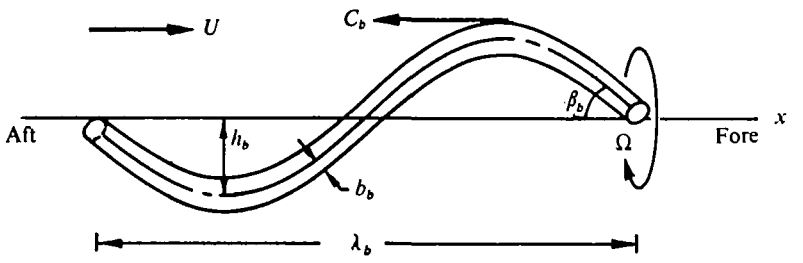

(*a*)

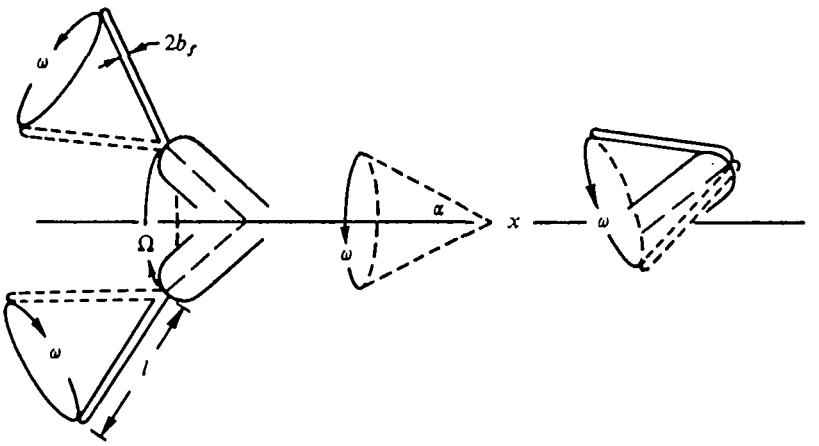

(*b*)

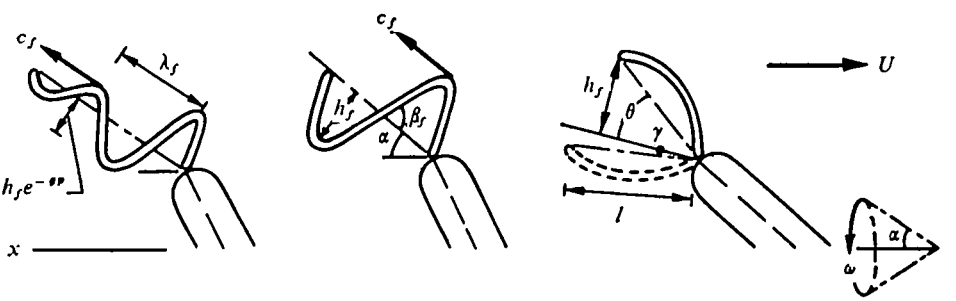

(*c*)

Fig. 2. The kinematic parameters associated with the rigid helical *Spirillum* body (*a*), the conical beat bundle C (*b*), the damped helical beat bundle DH (*c*, first diagram), the rigid helical beat bundle RH (*c*, second diagram) and the parabolic beat bundle PB (*c*, third diagram). The directions of wave propagation (c_b and c_f) and rotation (ω and Ω) are shown in each case. In all cases save the conical bundle model α at any instant is formed by an imaginary axis (straight broken lines) with the x axis. For the C the angle-forming axis is the bundle material axis.

balanced, the organism moves forward (in the positive x direction) at a constant velocity U. The resulting swimming is called quasi-steady (because oscillations are present but relatively small as determined by the oscillatory Reynolds number $\mathrm{Re}_w = fl^2/v$ which is $\ll 1$) and characterizes all motion which conforms to rotational resistive theory.

In the CWW model the function of the flagellar bundle is limited to the production of ω as it is taken to transcribe a cone of half-angle α with the x axis. Implicit in this assumption is a limitation of flexibility in the bundle to a small region near the base. The alternative to bundle flexibility would be a single rotating shaft which is not conceivable for the bundle as a unit because each of its individual flagella arise from separate 'holes' in the cell wall (Williams & Chapman, 1961) and it is unlikely that all but one of the entire array of flagella can detach themselves from their moorings and revolve around the flagellum remaining attached. This view of the bundle beat is similar to that of Metzner (1921) with the added simplification of an unbent distal bundle end.

It is the purpose of this report to show that (1) the bundles are bent distally and (2) at least one of the bundles contributes directly to the balanced force component of the swimming bacterium by propagating a helical (or at least three-dimensional) wave of velocity $c_f = \omega/k_f$ (where $k_f = 2\pi/\lambda_f$) and that the aft (posterior) bundle is the more likely candidate for this beat form.

METHODS AND MATERIALS

Observations

Spirillum volutans was obtained from the American Type Culture collection (catalogue No. 19553) and a bacterium assumed to be the same species was collected from Los Angeles hyperion (sewage treatment) plant sludge. The organisms were maintained without aeration at room temperature (21–25 °C) until use, whereupon they were allowed to cool to 20 °C.

Spirilla to be analysed were suspended in a petroleum jelly-ringed slide preparation and photographed with a Milliken DBM-55 cine camera at speeds of 100–300 frames/s. Darkfield illumination was provided by a camera-pulsed xenon-arc lamp. Magnification was provided by a Zeiss WL microscope system fitted with a darkfield Apo 40 × objective. The resulting films were analysed through tracings made on a parallax-corrected Triad film reader. All observations and recordings were made at 20 °C. To ensure that organisms photographed were not unevenly influenced by wall drag, the plane of focus was maintained midway between the coverslip and the slide. One cannot assume, of course, that all wall effects were eliminated.

A total of 18 Spirilla were analysed. All motions were referenced to the lab system. Values for c_b and c_f were determined by direct measurement of wave progression or by following the progress of illuminated spots on the wave which were formed when the curved structure moved into and out of the darkfield light belt. Time measurements were facilitated by a timing light in the camera which marked the film at 120 Hz. Values for Ω and ω were determined by three complementary methods. First from rotation frequency measurements obtained from the films where, $\Omega = 2\pi f_b$ and $\omega = 2\pi f_f$ (with f_b and f_f the body and flagellar bundle frequencies respectively). Second, from c_b and c_f, utilizing the definitions given above. Third, the general range for Ω was verified by direct observation of swimming Spirilla wherein the regular xenon-arc was replaced by

a Strobotac (General Radio) and the flash rate was decreased slowly from 600 Hz to the values at which the body appeared as two standing wave images 180° out of phase, and then one standing wave image. The value of Ω obtained in this manner was then compared with measurements from the first two methods. If the range of values agreed, the original measurements were considered verified.

Diagrams showing the parameters measured for each model are presented in Fig. 2. All symbols with '*b*' subscripts refer to the rigid body and all symbols with '*f*' subscripts to the flagellar bundles regardless of their geometry. The measurements indicated in Fig. 2(*a*) are straightforward and easy to obtain. The quantity β_b which is the helical pitch angle is readily calculated from $\tan \beta_b = k_b h_b$.

The most difficult measurement to evaluate is α, the average angle formed by the bundle with the progression or x axis. The reasons for this difficulty are clear from Fig. 2(*b*). As the body helix rotates it carries the axis of the bundle beat around and it is unlikely that this axis is a linear extension of the body material axis (the long dash line in figure) because during the forward motion of the organism the bundles are bent aftward by viscous drag; however, calculations are greatly simplified if we ignore this difference. Couple this condition with the fact that ω is always greater than Ω and it becomes clear that any representative value for α must be an average. In addition, the α observed through the microscope is a projection of the true three-dimensional angle onto the plane of view, so the only hope for obtaining a true value for any instantaneous α is limited to the instant when the tip of the body helix and the tip of the bundle emerging from it move into the plane of view simultaneously. Accordingly, α is represented by a range of values which is approximated from the maximum and minimum measured values and for calculations we make the further simplification that the flagellar bundle axis coincides with the body material axis as in Fig. 1.

Fig. 2(*c*) summarizes the bundle beat models to be matched against the conical beat model of 2(*b*). At the left the damped helix DH, at the centre the rigid helix RH and at the right the parabola PB. In all applications of the models the values of h_f and λ_f chosen as constants were single values obtained from one organism swimming at an average velocity (note that $\tan \beta_f = h_f k_f$). For the parabolic beat an estimate of the focus γ was obtained from $\gamma = 0{\cdot}25 h_f^2 (l^2 - h_f^2)^{-\frac{1}{2}}$ where h_f and $l = 7\,\mu$m, the approximate bundle length (Metzner, 1921), form two sides of a right triangle as illustrated in the third diagram of Fig. 2(*c*).

Representation of the motion – kinematics

Three bundle motion geometries were examined *vis-à-vis* the conical beat form. In the simplest the bundle was allowed to possess sufficient flexibility to be bent into a parabola by the viscous drag on the swimming organism. The other two geometries were both helical; one replacing the stiff portion of the unbent bundle with a rigid helical bundle and the other replacing the stiff portion with a flexible helix which is assumed to have passive flexibility. Accordingly, the flexible helix would have to express the damping effects of viscous drag. Note that since resistive theory assumes quasi-steady motion there is no allowance for time-dependent variations in either wave propagation or rotation about the material axis of a flagellar bundle. Accordingly, the fluid does not 'recognize' a bundle's 'elastic' events beyond their expression in the form of the bundle wave. The form of the wave, in turn, becomes the only basis by which bundle

elasticity may be measured (it is a parameter of the damping factor g which is discussed below). The significance of the quasi-steady assumption is evident in the small differences between the damped and flexible helix bundle models to be presented below (such differences become large only when $g \ll 1$ or $g \gg 1$, conditions which are not explored because they are not supported by observation).

The geometry of a parabolic bundle may be stated in Cartesian notation as $z^2+y^2 = 4\gamma x$. If we take $q = -x$ as a parameter along the x axis, then we obtain for the *body* reference system

$$x = -q, \quad y = 2(\gamma q)^{\frac{1}{2}} \sin\phi, \quad z = 2(\gamma q)^{\frac{1}{2}} \cos\phi, \quad 0 \leqslant q \leqslant l, \tag{2}$$

where $\phi = \omega t$ (t is time). Since the organism is swimming at a velocity U along the x axis, any given element of the bundle will be found at any instant after $t = 0$ to be at $Ut-q$ in the *lab* reference system and the parametric vector form for the motion geometry will be

$$\mathbf{r}_p = (Ut-q)\,\mathbf{i} + 2(\gamma q)^{\frac{1}{2}} \sin\phi\,\mathbf{j} + 2(\gamma q)^{\frac{1}{2}} \cos\phi\,\mathbf{k}. \tag{3}$$

By a similar argument we have for the rigid circular helix wave

$$\mathbf{r}_r = (Ut-p)\,\mathbf{i} + h_f \sin\theta\,\mathbf{j} + h_f \cos\theta\,\mathbf{k}, \quad 0 \leqslant p \leqslant n_f \lambda_f, \tag{4}$$

with $p = x$ the parameter in the body reference frame and $\theta = k_f p + \omega t$. For the damped bundle the waves were taken to be damped in the y and z directions with the damping coefficient e^{-gp}. Here g is the damping factor with $g > 0$ and p is taken to be the same parameter as before. If we make the further simplifying assumption that k_f remains constant then (4) becomes

$$\mathbf{r}_d = (Ut-p)\,\mathbf{i} + e^{-gp} h_f \sin\theta\,\mathbf{j} + e^{-gp} h_f \cos\theta\,\mathbf{k}, \quad (0 \leqslant p \leqslant n_f \lambda_f, \quad g > 0) \tag{5}$$

for the damped helical bundle.

The rigid helical body will conform to the same geometry as the rigid bundle so its parametric vector form will be

$$\mathbf{r}_b = (Ut+w)\,\mathbf{i} + h_b \sin\Theta\,\mathbf{j} + h_b \cos\Theta\,\mathbf{k}, \quad 0 \leqslant w \leqslant n_b \lambda_b \tag{6}$$

with w, x the parameter in the body reference frame and $\Theta = k_b w - \Omega t$, where Ω is negative because the body must rotate in a sense opposite that of the bundles. (note c_b must remain in the same sense as c_f, so we have $c_b k_b = -\Omega$).

Forces generated by the motion – dynamics

The forces generated by the given swimming geometries are obtained directly after substitution of equations (3–6) into appendix equation (A7).

$$dF_b = [U(C_s - C_n A_b) + c_b C_s \kappa_b^2]\, A_b^{-\frac{1}{2}}\, dw. \tag{7}$$

$$dF_p = Um\,[C_s'(\gamma q)^{\frac{1}{2}} B^{-1} - C_n'(\gamma q)^{-\frac{1}{2}} B] \cos\alpha\, dq. \tag{8}$$

$$dF_r = -m[U(C_n' A_f - C_s') + c_f C_s' \kappa_f^2]\, A_f^{-\frac{1}{2}} \cos\alpha\, dp. \tag{9}$$

$$dF_d = -m[U(C_n' D - C_s') + c_f C_s' \kappa_f^2\, e^{-2gp}]\, D^{-\frac{1}{2}} \cos\alpha\, dp \tag{10}$$

where m is the number of bundles $A_b = 1+\kappa_b^2$, $A_f = 1+\kappa_f^2$, $B = (\gamma q+1)^{\frac{1}{2}}$, and $D = (1+a^2 e^{-2gp})$ with $a^2 = h_f^2(g^2+k_f^2)$;* and it is understood that only the x-component of each force is utilized (the $\cos\alpha$ terms project the off-axis bundle beat onto the x axis).

* Dummy variables are used for all differential equations and should be thought of as being automatically replaced by the limits of (11–13) after integration (i.e. w becomes $n_b \lambda_b$, q becomes l and p becomes $n_f \lambda_f$)

Table 1. *Geometric quantities of swimming* Spirillum

(All variances are sample standard deviations. The quantities b_f and b_f upon which the viscous force coefficients are based were obtained from (1) (Strength & Krieg, 1971). All symbols are defined in the text.)

Quantity	Average value	Value range
b_b	—	$(0{\cdot}7-0{\cdot}85)\times10^{-4}$ cm (1)
n_b	$2{\cdot}15\pm0{\cdot}6$	$1{\cdot}16-3{\cdot}20$
λ_b	$(13{\cdot}2\pm2{\cdot}0)\times10^{-4}$ cm	$(8{\cdot}5-17{\cdot}3)\times10^{-4}$ cm
h_b	$(1{\cdot}51\pm0{\cdot}48)\times10^{-4}$ cm	$(0{\cdot}78-2{\cdot}50)\times10^{-4}$ cm
C_n	$0{\cdot}1109\pm0{\cdot}0170$	$0{\cdot}0619-0{\cdot}1430$ (1)
C_s	$0{\cdot}1024\pm0{\cdot}0266$	$0{\cdot}0411-0{\cdot}1658$
C_m	—	$(6{\cdot}2-9{\cdot}1)\times10^{-10}$
b_f	—	$(0{\cdot}13-0{\cdot}15)\times10^{-4}$ cm (1)
n_f	$1{\cdot}11$	—
λ_f	$6{\cdot}5\times10^{-4}$ cm	—
h_f	$1{\cdot}47\times10^{-4}$ cm	—
C'_n DH	—	$0{\cdot}0440-0{\cdot}0651$
PB	$0{\cdot}0081$	—
RH	—	$0{\cdot}0440-0{\cdot}0651$
C(CWW)	$0{\cdot}0784$	—
C'_s DH	—	$0{\cdot}0350-0{\cdot}0547$
PB	$0{\cdot}0042$	—
RH	—	$0{\cdot}0350-0{\cdot}0547$
C(CWW)	$0{\cdot}0569$	—
C'_m	—	$(2{\cdot}1-2{\cdot}8)\times10^{-11}$
α	—	$11{\cdot}4-53{\cdot}0$

The balanced force equations are formed by adding (7) to each of (8–10) and setting all three integrated force sums equal to zero:

$$\int_0^{l \text{ and } n_b\lambda_b}[dF_b+dF_p]=0, \tag{11}$$

$$\int_0^{n\lambda}[dF_b+dF_r]=0, \tag{12}$$

$$\int_0^{n\lambda}[dF_b+dF_d]=0. \tag{13}$$

If both a fore and an aft bundle are present the bundle forces are multiplied by two ($m=2$). If, however, the fore and aft bundle geometries differ, as in the case of a parabolic fore bundle and a damped helical aft bundle, then the total force on the organism is the sum of three forces

$$\int[dF_b+dF_p+dF_d]=0. \tag{14}$$

Similarly, the torques or moments of force about the x axis on each of the four structures are obtained directly after substitution of equations (3–6) into appendix equation (A 10). The momentum statement can be simplified by noting that C_s and $C'_s \gg C_m$ and C'_m for Spirillum as indicated in Table 1. Accordingly, we drop the C_m and C'_m terms and obtain

$$dM_b\,\mathbf{i}=-h_b[\Omega h_b(C_nA_b-C_s\kappa_b^2)+UC_s\kappa_b]A_b^{-\frac{1}{2}}\,dw\mathbf{i}. \tag{15}$$

$$dM_p\,\mathbf{i}=4\omega C'_n\,m(\gamma q)^{\frac{1}{2}}B\cos\alpha\,dq\mathbf{i}. \tag{16}$$

$$dM_r\,\mathbf{i}=mh_f[\omega h_f(C'_nA_f-C'_s\kappa_f^2)+UC'_s\kappa_f]A_f^{-\frac{1}{2}}\cos\alpha\,dp\mathbf{i} \tag{17}$$

$$dM_d\,\mathbf{i}=mh_f[\omega h_f(C'_nD-C'_s\kappa_f^2\,e^{-2pq})+UC'_s\kappa_f]D^{-\frac{1}{2}}e^{-2pq}\cos\alpha\,dp\mathbf{i}. \tag{18}$$

Table 2. *Model velocity ratios*

Model	Ratio	Where	Eqn. no.
PB (parabola)	$\frac{U}{c_b} = \frac{k_b B_1}{P_1 - B_2}$	$\begin{cases} B_1 = (C_n - C_s) n_b \lambda_b h_b \kappa_b A_b^{-\frac{1}{2}} \\ B_2 = n_b \lambda_b ((C_n - C_s) - C_n A_b) A_b^{-\frac{1}{2}} \\ P_1 = m\gamma^{-1}(C'_n P_3 - (C'_n - C'_s) P_2) \cos\alpha \\ P_2 = (\gamma l)^{\frac{1}{2}} B + \ln[(\gamma l)^{\frac{1}{2}} + B] \\ P_3 = (\gamma l)^{\frac{1}{2}} B - \ln[(\gamma l)^{\frac{1}{2}} + B] \end{cases}$	(23)
RH (rigid helix)	$\frac{U}{c_b k_b B_1 - c_f k_f R_1} = \frac{1}{R_2 - B_2}$	$\begin{cases} R_1 = (C'_n - C'_s) m n_f \lambda_f h_f k_f A_f^{-\frac{1}{2}} \cos\alpha \\ R_2 = m n_f \lambda_f (C'_n A_f - (C'_n - C'_s)) A_f^{-\frac{1}{2}} \cos\alpha \end{cases}$	(24)
DH (damped helix)	$\frac{U}{c_b k B_1 + c_f k_f D_1} = \frac{1}{D_2 - B_2}$	$\begin{cases} D_1 = (C'_n - C'_s) m h_f a^{-2} g^{-1} \kappa_f D_3 \cos\alpha \\ D_2 = \mathrm{mg}^{-1}[C'_n D_3 + \frac{1}{2} - C'_s D_4] \cos\alpha \\ D_3 = (1 + a^2)^{\frac{1}{2}} - D^{\frac{1}{2}} \\ D_4 = \ln\left[\frac{\sqrt{(1+a^2)} - 1}{\sqrt{(1+a^2)} + 1}\right] - \ln\left[\frac{D^{\frac{1}{2}} - 1}{D^{\frac{1}{2}} + 1}\right] \end{cases}$	(25)
DHPB (fore parabola – aft damped helix)	$\frac{U}{c_b k_b B_1 + c_f k_f D_1} = \frac{1}{D_2 - B_2 + P_1}$	See above	(26)

Table 3. *Model spin ratios*

Model	$\Omega/\omega =$	Where	Eqn. no.
PB (parabola)	$\frac{P_4 (P_1 - B_2)}{B_2 (P_1 - B_2) - B_1^2}$	$\begin{cases} B_2 = n_b \lambda_b h_b^2 (C_n A_b - (C_n - C_s \kappa_b^2) A_b^{-\frac{1}{2}} \\ P_4 = C'_n m \gamma^{-1} [(\gamma l)^{\frac{1}{2}} B P_5 - \frac{1}{2} P_6] \cos\alpha \\ P_5 = 2\gamma l + 1 \\ P_6 = \ln[P_5 + 2(\gamma l)^{\frac{1}{2}} B] \end{cases}$	(27)
RH (rigid helix)	$\frac{R_1 (B_1 - R_1) + R_2 (R_2 - B_2)}{B_1 (B_1 - R_1) + B_2 (R_2 - B_2)}$	$R_2 = m n_f \lambda_f h_f^2 (C'_n A_f - (C_n - C'_s) \kappa_f^2) A_f^{-\frac{1}{2}} \cos\alpha$	(28)
DH (damped helix)	$\frac{D_1 (B_1 + D_1) + D_2 (B_2 - D_2)}{B_1 (B_1 + D_1) + B_2 (B_2 - D_2)}$	$\begin{cases} D_2 = m a^{-2} g^{-1} h_f^2 [C'_n D_3 + a^{-2} (C'_n a^2 - (C'_n - C'_s) \kappa_f^2) (D_3 - D_4)] \cos\alpha \\ D_4 = \frac{1}{3}[1 + a^2)^{1.5} - D^{1.5}] \end{cases}$	(29)
DHPB (fore parabola – aft damped helix)	$\frac{D_1 (B_1 + D_1) - (D_2 + P_4) (P_1 - B_2 + D_2)}{B_1 (B_1 + D_1) - B_2 (P_1 - B_2 + D_2)}$	See above	(30)

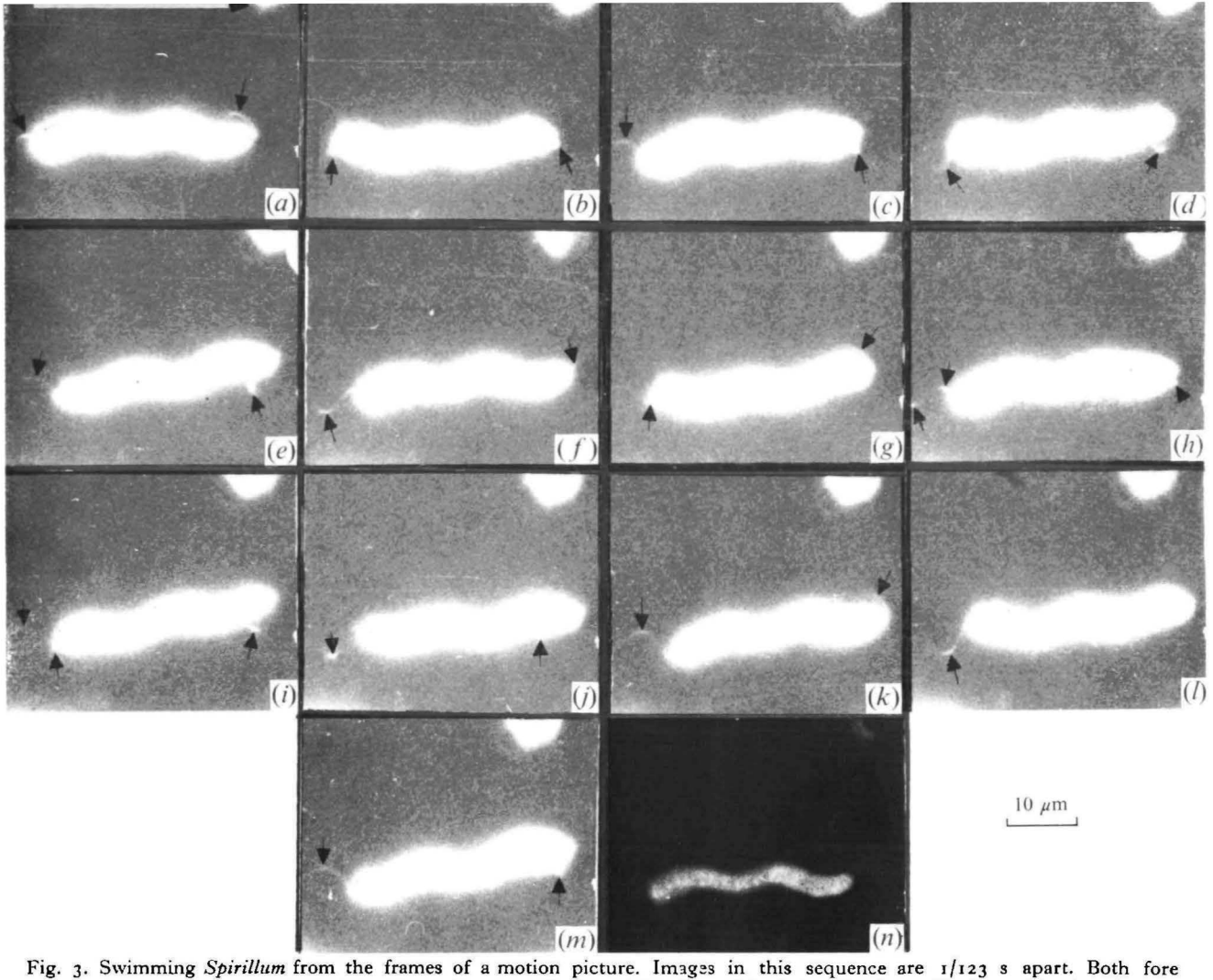

Fig. 3. Swimming *Spirillum* from the frames of a motion picture. Images in this sequence are 1/123 s apart. Both fore and aft flagellar bundles are indicated with small arrows Backward bending of both bundles is readily detectable; in addition, the distal ends are bent (see *c*, *d*, *e*, *f*, *j*, *k*, *l* and *m*), an observation not in agreement with the CWW model. The large arrow in (*a*) indicates translational direction.

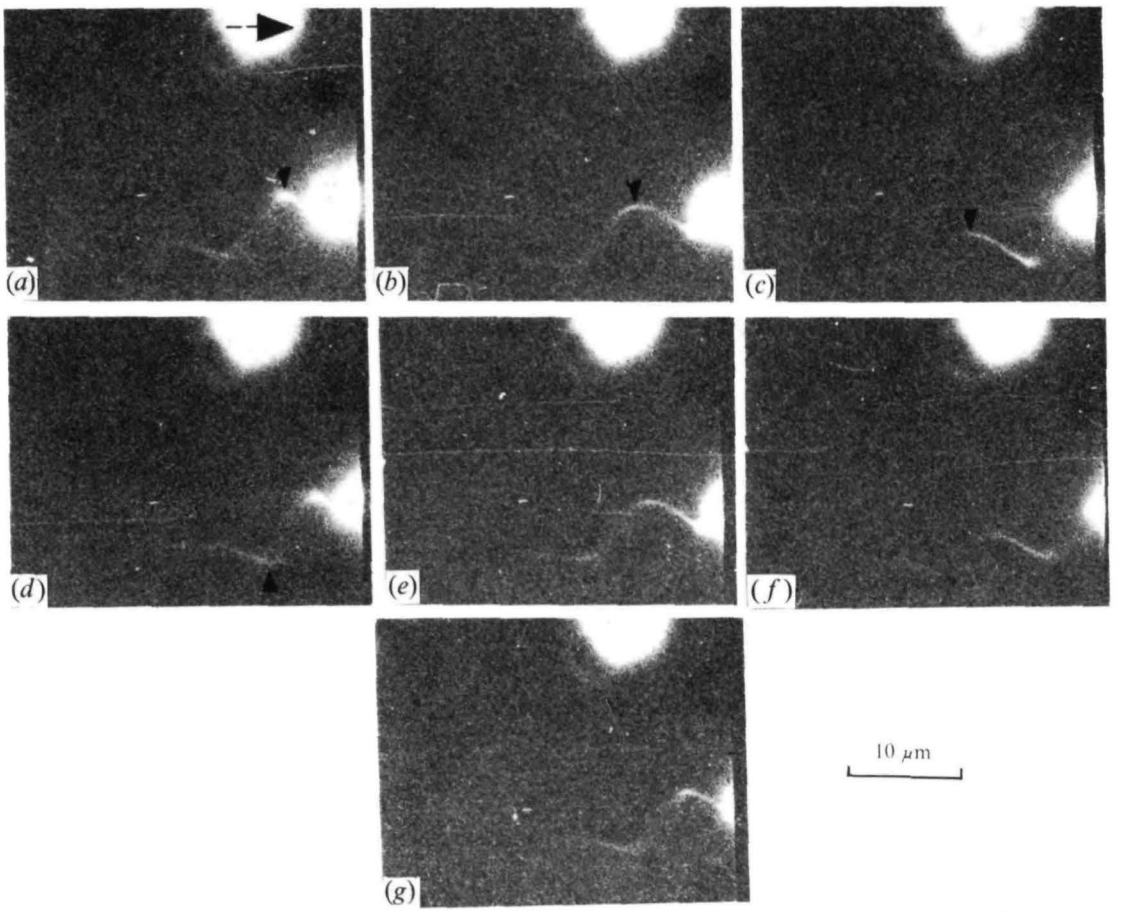

Fig. 4. Three-dimensional wave propagation along an aft flagellar bundle of a swimming *Spirillum*. The three-dimensional character of the wave is detectable from the in-light and out-of-light or in-focus and out-of-focus alternations along the bundle (see especially *a*, *d* and *e*). Images are 1/123 s apart.

The balanced torque equations are formed by adding (15) to each of (16–18) and integrating over the entire organism to obtain the net zero statements:

$$\int_0^{l \text{ and } n_b \lambda_b} [dM_b + dM_p] = 0, \tag{19}$$

$$\int_0^{n\lambda} [dM_b + dM_r] = 0, \tag{20}$$

$$\int_0^{n\lambda} [dM_b + dM_d] = 0. \tag{21}$$

Continuing the same pattern used for the balanced force equations, we double the bundle torque terms if the organism has bipolar bundles and if the bundle geometries match those of (14) we have

$$\int [dM_b + dM_p + dM_d] = 0. \tag{22}$$

Testing of the models – velocity and spin ratios

In measuring the degree to which each model fits observations one can often take advantage of the linearity of (11–14) and (19–22) to separate the velocity from the geometric terms. The ideal resulting statements are of the form U/c (velocity ratio) and Ω/ω (spin ratio). Where c_b the body wave propagation velocity and c_f the bundle wave propagation velocity are both present, separation is less than ideal but by solving for U, substituting the answer in the balanced torque equation and utilizing the definitions of Ω the body angular velocity and ω the bundle angular velocity, the spin terms can still be retained in the form Ω/ω (the U and c term is, in any case, called a 'velocity ratio'). Accordingly, the velocity and spin ratios for each of the models are presented in Tables 2 and 3.

RESULTS

The traditional notion of the *Spirillum* swimming form is illustrated in the cine film sequence of Fig. 3. The swept-back appearance of both bundles conforms more to the parabolic arcs in Metzner's (1921) drawings than to the straight rod of the CWW model (which, as we shall see, is nevertheless a reasonable approximation). Such observed geometry is consistent with the expected curvature for a real attached fibre being bent back under a uniform stress.

One can appreciate the acceptability of Metzner's interpretation when the available data consistently confirm his observations. If, however, one makes a long exposure print of a film sequence showing the aft end of the swimming bacterium he obtains a bundle image as shown in Fig. 4 which is not unlike the three-dimensional bundlewave reported for compressed *Spirillum* by Jarosch (1972, his plate 14). Unfortunately, a similar print cannot be obtained for the fore end because the body reflects enough light to obscure the fore bundle. Notwithstanding this lack of data about the fore bundle, it is reasonable to assume that a beating flexible fore bundle has a geometry in the helix-to-parabola range. Tracings of the bundles carried by the specimen of Fig. 4 are presented in Fig. 5 and appear to bear this assumption out although the fore bundle is always incompletely represented. In any case, limitation of fore bundle geometry to a helix or a parabola and the aft bundle to a helix is reasonable given the data presented.

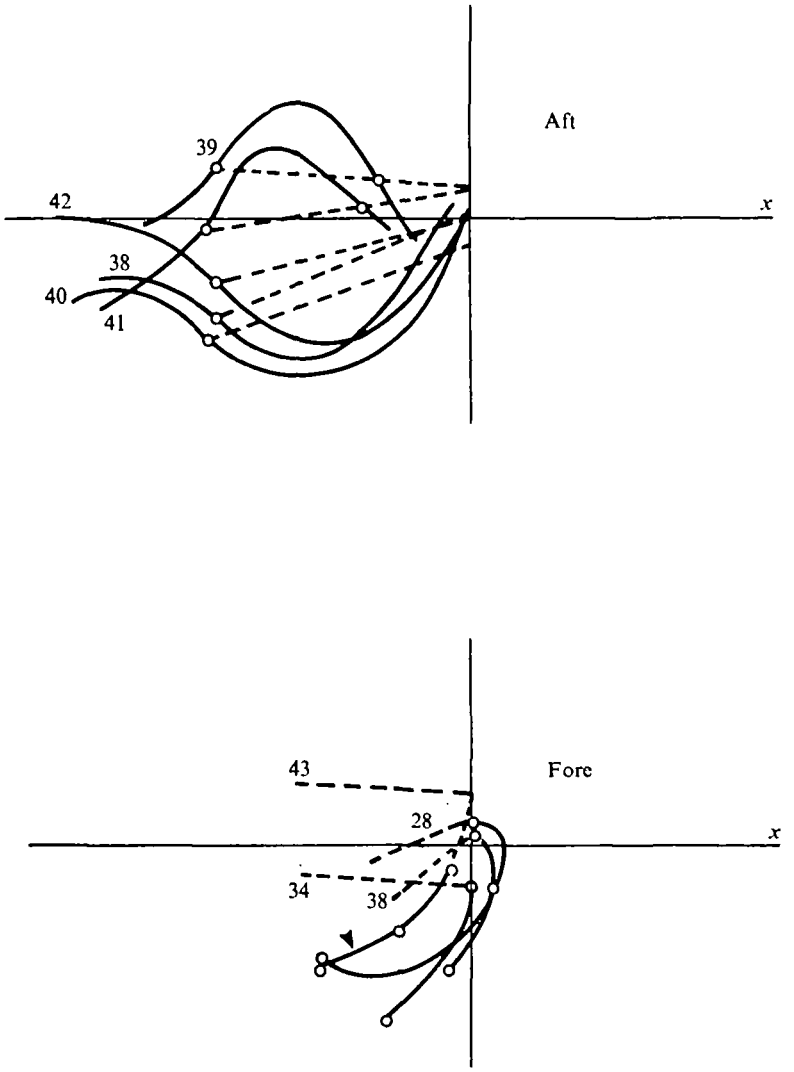

Fig. 5. Tracings from the bundle beat cycle of specimen shown in Fig. 4. The numbers shown indicate a frame number from the motion picture film and contiguous numbers are 1/123 seconds apart. The method for determining α from tracings like this is explained in the text. The off-translation axis characteristic of the bundle geometric axis is evident in this tracing. The dashed lines of the upper diagram – the aft bundle – are helical axes and those of the lower diagram – the fore bundle – are radii of curvature.

The models to be tested quantitatively against the CWW model are, then, the body with (1) one or two flexible (i.e. damped) helical bundles, or one flexible and/or one parabolic bundle (DHPB with appropriate choices for m), (2) one or two rigid helical bundles (RH) and – for completeness – (3) one or two parabolic bundles (PB).

The adaptability of rotational resistive theory is well illustrated in the DHPB model. Since the dynamic relationships for all models are composed of linear operators, one can superpose any two of them to get a combination model. Then one can test three models (e.g. a DH, a PB and a DHPB bundle) from the combination model by adjusting

Table 4. *Geometric parameters used to generate maxima and minima curves for the various bundle beat models*

The functions v and s are the velocity and spin ratios respectively. The focus γ and the body wavelength λ_b are given in cm. All symbols are defined in the text.)

		C(CWW)		DH		PB		DHPB		RH	
Parameter	Function	Min.	Max.	Min.	Max.	Min.	Max.	Min.	Max.	Min.	Max.
m	v	2	2	2	1	1	1	—	—	2	1
	s	2	2	2	2	1	1	—	—	2	2
κ_f	v	—	—	1·000	0·600	—	—	1·000	0·600	1·000	0·600
	s	—	—	1·000	1·200	—	—	1·000	1·200	1·500	1·200
cos α	v	0·597	0·597	0·597	0·980	0·980	0·597	0·980	0·597	0·597	0·980
	s	0·597	0·597	0·597	0·597	0·597	0·980	0·597	0·980	0·980	0·597
n_b	v	1·100	2·000	3·000	1·000	1·000	3·000	1·000	2·000	3·000	1·000
	s	1·100	2·000	3·000	2·000	3·000	2·000	3·000	2·000	2·000	2·000
λ_b	v	$5{\cdot}6\times10^{-3}$	$8{\cdot}5\times10^{-4}$	$2{\cdot}8\times10^{-3}$	$8{\cdot}5\times10^{-4}$	$8{\cdot}5\times10^{-4}$	$8{\cdot}5\times10^{-4}$	$8{\cdot}5\times10^{-4}$	$8{\cdot}5\times10^{-4}$	$2{\cdot}8\times10^{-3}$	$8{\cdot}5\times10^{-4}$
	s	$2{\cdot}8\times10^{-3}$	$8{\cdot}5\times10^{-4}$	$2{\cdot}5\times10^{-3}$	$8{\cdot}5\times10^{-4}$	$5{\cdot}6\times10^{-3}$	$2{\cdot}8\times10^{-3}$	$5{\cdot}6\times10^{-3}$	$2{\cdot}8\times10^{-3}$	$2{\cdot}8\times10^{-3}$	$8{\cdot}5\times10^{-4}$
Model specific		—		g		γ		γ/g		—	
	v			1·0	1·0	$5{\cdot}0\times10^{-3}$, $1{\cdot}6\times10^{-4}$		$6{\cdot}0\times10^{-3}/1{\cdot}0$, $6{\cdot}0\times10^{-3}/1{\cdot}0$			
	s			1·0	1·0	$6{\cdot}0\times10^{-3}$, $1{\cdot}6\times10^{-3}$		$6{\cdot}0\times10^{-3}/1{\cdot}0$, $1{\cdot}6\times10^{-3}/1{\cdot}0$			

m so that only terms for the model in question, and the number of bundles being considered, are present.

The curves which represent the various models and are compared with observations are all presented as functions of κ_b, a quantity which must be common to all possible models of *Spirillum*. Variation of κ_b, in turn, is due to changes in h_b as λ_b is limited to two values, one for generating higher and one for lower model curve values. Model curves generated by the right-hand side of the spin and velocity ratio equations for RH, DHPB, PB and C (from CWW) are compared with data points generated by the left-hand side of the same equations in Figs. 6 and 7. Each curve represents a maximum or minimum (not absolute) locus of values between which the measured ratios are supposed to lie. These extrema are not absolute because although they are maxima or minima for some of the parameters which generated them, they incorporate arbitrary estimates of such parameters as κ_f and g. Other quantities generating these curves were taken from the upper and lower ends of the ranges listed in Table 1. The specific values used to generate the extrema curves are listed in Table 4. All parameters were substituted into the right side of equations (23–30) to generate the curves presented in the figures. Measurements from 18 specimens were substituted into the left side of the same equations to obtain model test values. No value for c_f (and ω) could be obtained from six specimens. As nearly all of these had κ_b values near 1·0, an average spin ratio of 0·288 was obtained from an arbitrary selected group of specimens with κ_b values near 1·0 and this Ω/ω was used to generate the missing ω (and c_f) values from measured Ω body angular velocity values. The bundle parameters used in generating the data points of Fig. 6(a) are listed in Table 5. Averages and ranges for measured velocity and spin ratios are listed in Table 6. The large variances in the dynamic quantities are not surprising if one assumes that fine strands of debris connecting the organism with the slide are sufficient to result in lower-than-normal ratios. The highest ratios are not so easily explained, particularly when repeated examination of the original frames produced no evidence of convection. We may note in passing the rather large variance in κ_b.

Close examination of Figs. 6(a) and (b) reveals that all bundle beat forms save the parabolic are consistent with observations of swimming Spirilla. As indicated above, there are no time-dependent (i.e. elastic) hydrodynamic differences between the DH and RH models, but there are geometric dissimilarities which result from the elasticity disparity. The terms which express the geometric dissimilarities on the right side of equations (25) and (26) tend to be small and the resulting curves in Fig. 6(a) differ by less than 1 %. The left side of the same equation, however, contains c_f coefficients which magnify more than c_b coefficients. Accordingly, more discrepancy appears between the data points of Fig. 6(a). A number of data values appears outside the model ranges in both graphs of Fig. 6. The values below the minimum extremum can be readily explained as due to abnormally low U values which were probably caused by adherence of the organism to strands of debris (a likely complication in sewage samples) which may in turn be attached to the slide or coverslip. Data values above the maximum extremum cannot be so easily explained. As indicated above, fluid convection has not been detected and appears unlikely, given xenon strobe illumination and a petroleum jelly-sealed slide. One is intuitively suspicious of a high velocity ratio such as the U/c_b value of 0·96 for one $\kappa_b = 0{\cdot}738$. But repeated measurements of the recorded images produced

Table 5. *Geometric parameters used to calculate data points for the two helical bundle models, the damped helix DH and the rigid helix* RH

*The ω and c_f values for these specimens are estimated from $\Omega/\omega = 0{\cdot}288$.

		κ_f		$\cos\alpha$		C'_n		C'_s	
κ_b	m	DH	RH	DH	RH	DH	RH	DH	RH
0·371	1	0·600	0·750	0·980	0·597	0·0675	0·0651	0·0461	0·0439
0·460	1	1·000	1·000	0·597	0·597	0·0612	0·0612	0·0404	0·0404
0·512	2	1·200	2·500	0·597	0·980	0·0583	0·0466	0·0380	0·0286
0·537	2	1·200	1·500	0·597	0·980	0·0583	0·0547	0·0380	0·0350
0·574	2	1·200	1·200	0·597	0·597	0·0583	0·0583	0·0380	0·0380
0·586	2	1·200	1·200	0·597	0·597	0·0583	0·0583	0·0380	0·0380
0·738	2	0·600	0·750	0·980	0·597	0·0675	0·0651	0·0461	0·0439
0·738	2	0·750	0·750	0·597	0·597	0·0651	0·0651	0·0439	0·0439
0·819*	2	1·200	1·200	0·597	0·597	0·0583	0·0583	0·0380	0·0380
0·859*	1	1·000	1·000	0·597	0·597	0·0612	0·0612	0·0404	0·0404
0·889*	1	1·200	1·200	0·597	0·597	0·0583	0·0583	0·0380	0·0380
1·010	2	1·200	1·200	0·597	0·597	0·0583	0·0583	0·0380	0·0380
1·085	2	1·200	1·200	0·597	0·597	0·0583	0·0583	0·0380	0·0380
1·152*	2	1·200	1·500	0·597	0·980	0·0583	0·0612	0·0380	0·0404
1·157	1	0·600	0·750	0·980	0·597	0·0675	0·0651	0·0461	0·0439
1·190	2	1·000	1·000	0·597	0·597	0·0612	0·0612	0·0404	0·0404
1·432	2	1·500	3·000	0·980	0·980	0·0547	0·0466	0·0350	0·0286
1·626*	2	1·000	1·000	0·597	0·597	0·0612	0·0612	0·0404	0·0404

Table 6. *Measured velocity and spin ratios*

(The value of the body helical pitch tangent κ_b is included as a reference. All variances are standard deviations of the sample.)

Quantity	Sample	Average value	Value range
U/c_b	18	$0{\cdot}375 \pm 0{\cdot}256$	0·040–0·962
Ω/ω	12	$0{\cdot}375 \pm 0{\cdot}204$	0·158–0·755
κ_b	18	$0{\cdot}874 \pm 0{\cdot}350$	0·371–1·626

no other value. Moreover, the present value does fit the helical models, so its existence cannot be dismissed out of hand as anomalous. Other velocity ratio data points which are significantly underestimated by model ranges may be found to lie above the PB maximum extremum curve, and, as expected, above the DHPB curves whose extrema are both too small *vis-à-vis* the data.

All spin ratio plots are referenced to the same Ω/ω form of spin ratio so a direct comparison can be made of the four basic models. It is difficult to imagine data which would exceed the extrema of all but the PB and DHPB plots. Thus, it is not surprising that no data points fall outside the C, DH or RH extrema. Moreover, the points which lie outside the two sets of PB plots are below their estimated value, a condition which can be explained by the same reasoning as that presented for the similar condition in the velocity ratio plots.

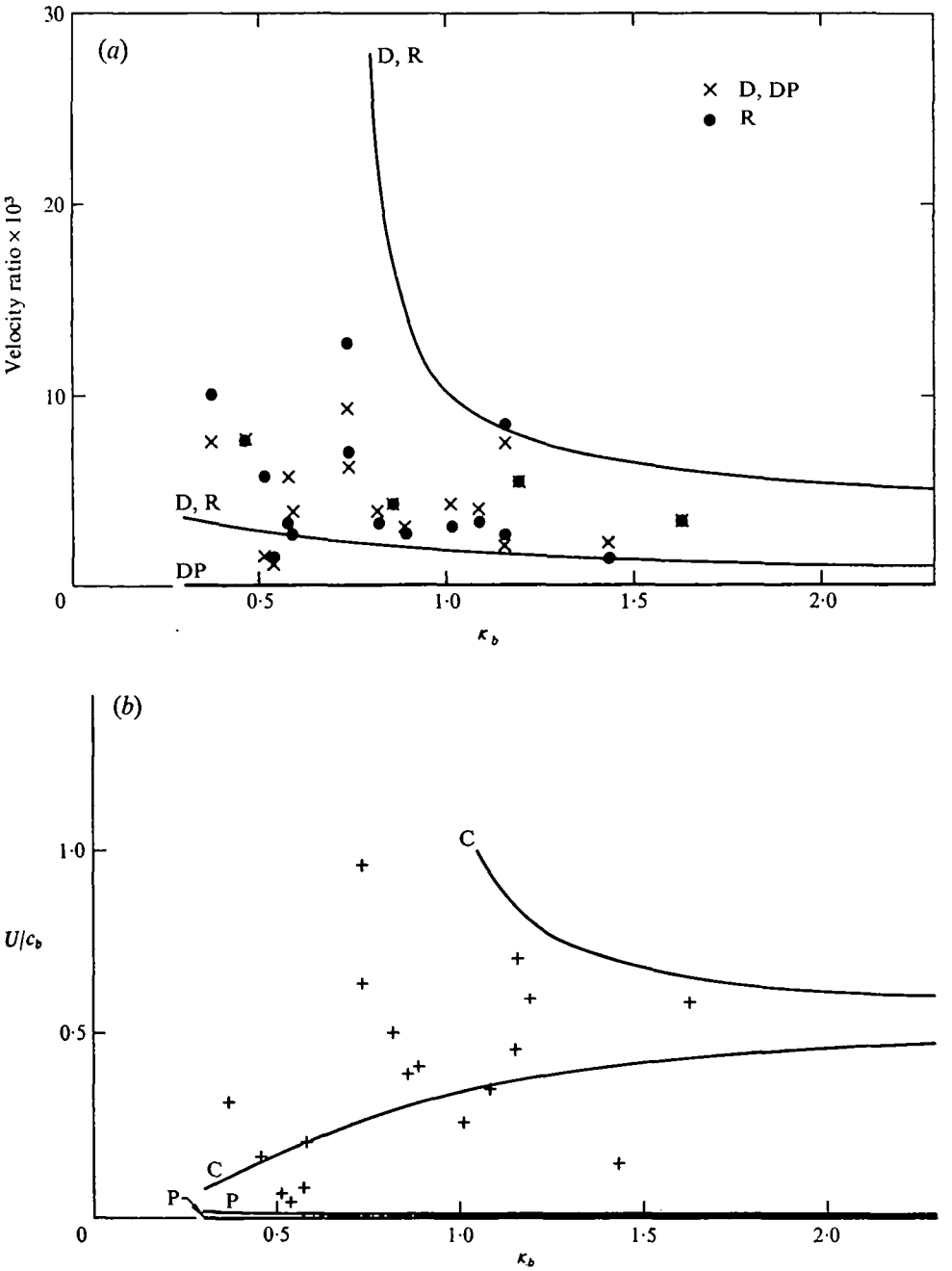

Fig. 6. Velocity ratios as functions of body helix pitch. Model symbols have been shortened for convenience, from DH to D, from RH to R, from PB to P, from DHPB to DP and from CWW to C. The parameters used to generate the 'extrema' model curves are listed in Table 4. The parameters used to generate the data points are listed in Table 5.

CONCLUSIONS

Observed spin and velocity ratios remain within the presented limits for all models of Spirillum swimming save those which include the PB geometry (see Figs. 6, 7). While PB-containing models performed acceptably in predicting spin ratios, they consistently underestimated the observed velocity ratios. The PB models, then, are invalidated by their predicted velocity ratios, notwithstanding the observations of Metzner (1921). The CWW model, in turn, is invalidated by photographic evidence, so, the accuracy of its theoretical dynamic ratio predictions must be considered fortuitous.

There remain, then, the two helical models which differ so slightly in their ability to account for the data that one cannot choose between them. The true bundle wave may, in fact, be between 'rigid' and 'flexible' because there is evidence supporting both extremes. On the one hand there must be enough flexibility to allow for the rather high curvature bends near the base of the fore bundle which are detectable in Fig. 3 (*a*, *d*, *g*). The curling of individual flagella of a rod bacterium bearing bipolar bundles as described by Strength & Kreig (1971) also suggests a less-than-rigid flagellar structure. Given a flexible bundle one would expect, of course, that upon making the 'decision' to swim, a Spirillum commences a whipping motion with both bundles which would propagate a base-to-tip helical wave down each. The firings of the initial beat impulses at the two bundles would have to be asynchonous and/or of unequal magnitude – a likely condition given an anisotropic stimulus such as a chemical diffusion gradient – such that one of the two bundles would assume the lead in accelerating to a maximum ω, angular velocity. Since both bundles naturally point away from the transverse plane of the body (see Fig. 2), the lead bundle would become the aft bundle and as the body attains steady translation the viscous stresses would bend both bundles aftward in a manner similar to that detectable in Figs. 3 and 5. Implicit in this interpretation is the prediction that a monotrichous Spirillum has an aft bundle only.

On the other hand, there must be limits to flagellar flexibility which would account for the observations of Jarosch (1972) cited above that the flagella of bundles splayed out by flattening *Spirillum* do not exhibit the pronounced damping one would expect for a flexible body, particularly one near a wall. Nor would flexibility be consistent with the report of Krieg, Tomelty & Wells (1967) that the bundles (which they term 'fascicles') of non-translating *Spirillum volutans* treated with coordination inhibitors rotate as mirror images of one another.

The effect of viscous bending on the motion of the individual flagella is not clear. The rotating shaft concept of flagellar beat generation (Doetsch, 1966; Mussill & Jarosch, 1972; Berg & Anderson, 1973) is certainly supported by the observations that individual flagella arise from separate 'holes' in the cell membrane (Williams & Chapman, 1961) and the observation that the cell body of a bacterium stuck to a glass slide by its bundle 'would undergo violent back-and-forth movements around the point of attachment' (Strength & Krieg, 1971). Moreover, there is no basis for assuming any incompatability in accepting both an RH bundle and an individual flagellum rotation model so long as the flagella are wound in a sense opposite that of their rotation (Smith & Koffler, 1971). There is, however, some evidence that the flagella of *Spirillum*-like bacteria – at least *Spirillum serpens* – arise from a single common basal structure (Abram, 1969 as cited by Smith & Koffler, 1971). If the basal ends of all the flagella are

DISCUSSION

Power expenditures for Spirillum swimming

Each living organism has at any instant a limited supply of biochemical energy which is dissipated in the performance of chemical, mechanical, and concentration work. The mechanical work performed by a bacterium is limited to flagellar motion (with a possible exception being a flexibacterium) which is divided into work performed against elastic (internal) and work performed against hydrodynamic (external) resistance. Elastic resistance includes 'bearing friction' on the rotating flagellum and the stiffness of the flagellum as it relates to wave propagation. The latter is, of course, negligible in an RH-type flagellum. (As regards the stiffness of the bundle, we can say that the fact that *Spirillum* can reverse its swimming direction precludes a rigid-helix-parabola combination which would be inconsistent with the exchange of bundle geometries between the poles which should accompany swimming reversal.)

Hydrodynamic resistance includes not only the viscous stresses upon which rotation resistive theory is based, but also the viscous and pressure stresses which may develop because of the non-slip condition at each solid boundary of two flagella which rotate very close to one another. Berg & Anderson (1973) estimate that the value of this inter-flagellar drag is small because the spacing of the flagellar array is relatively large, but the actual spacing of the flagella has not been measured and dynamic pressure can be considerable where moving bodies are close enough to require a lubrication theory motion analysis. Hence, the question of the significance of inter-flagellar energy dissipation cannot be considered settled.

Since the present analysis is confined to the net motion of the bundle, estimation of the rate of dissipation by or rate of work performed against the fluid viscous resistance during swimming is relatively simple. The power exerted by a swimming Spirillum against fluid resistance may be calculated for the models considered in this report by substituting (3–6) into (A 13) to obtain for the rigid helical body,

$$dP_b = [C_n(U^2+\Omega^2 h_b^2)A_b - C_s(U-\Omega h_b\kappa_b)^2]\,A_b^{-\frac{1}{2}}\,dw; \tag{31}$$

for m PB bundles,

$$dP_p = m\{U^2[C_n' B(\gamma q)^{-\frac{1}{2}} - C_s' B^{-1}(\gamma q)^{\frac{1}{2}}] + 4\omega^2 C_n' B(\gamma q)^{\frac{1}{2}}\}\cos\alpha\,dq; \tag{32}$$

for m RH bundles,

$$dP_r = m[U^2(C_n' A_f - C_s') + \omega^2 h_f^2(C_n' A_f - C_s'\kappa_f^2) + 2C_s' U\omega h_f\kappa_f]\cos\alpha\,dp; \tag{33}$$

and for m DH bundles,

$$dP_d = m[U^2(C_n' - C_s') + (C_n'\omega^2 h_f^2 + C_n' U^2 a^2 + 2C_s' U\omega h_f\kappa_f)\,e^{-2\sigma p} + \omega^2 h_f^2(C_n' a^2 - C_s'\kappa_f^2)\,e^{-4\sigma p}]\,D^{-1}\cos\alpha\,dp. \tag{34}$$

Integration of (31–34) over the entire body or bundle length gives for these models the expressions listed in Table 7.

Accordingly, the total power output against viscous resistance by Spirilla swimming with one of the four basic bundle geometries considered here is, for the PB model

$$P_{\mathrm{PB}} = P_b + P_p \tag{39}$$

for the RH model

$$P_{\mathrm{RH}} = P_b + P_r \tag{40}$$

Table 7. *Power dissipated against fluid resistance to propulsion*

Model	Power	Where	Equation no.
Rigid helical body	$-P_b = n_b \lambda_b [C_n(U^2+\Omega^2 h_b^2) A_b - (C_n - C_s)(U-\Omega h_b \kappa_b)^2] A_b^{-\frac{1}{2}}$		(35)
PB (parabola)	$-P_p = m\gamma^{-1}\{U^2[C_n'(N_1+N_2)-(C-C_s')(N_1N_3)] + \omega^2 C_n'(N_3-\frac{1}{2}N_4)\}\cos\alpha$	$\begin{cases} N_1 = (\gamma l)^{\frac{1}{2}} B \\ N_2 = \ln[(\gamma l)^{\frac{1}{2}}+B] \\ N_3 = (2\gamma l+1)N_1 \\ N_4 = \ln[(2l+1)+2N_1] \end{cases}$	(36)
RH (rigid helix)	$-P_r = mn_f \lambda_f (U^2 H_1 + \omega^2 H_2 + 2U\omega H_3) A^{-\frac{1}{2}} \cos\alpha$	$\begin{cases} H_1 = C_n' A_f - (C_n' - C_s') \\ H_2 = h_f^2 (C_n' A_f - (C_n' - C_s')\kappa_f^2) \\ H_3 = (C_n' - C_s') h_f \kappa_f \end{cases}$	(37)
DH (damped helix)	$-P_d = mg^{-1}(U^2 \mathcal{J}_2 + \omega^2 \mathcal{J}_3 + 2U\omega \mathcal{J}_4) D^{-\frac{1}{2}} \cos\alpha$	$\begin{cases} \mathcal{J}_1 = (1+a^2) \\ \mathcal{J}_2 = C_n'(\mathcal{J}_1^{\frac{1}{2}} - D^{\frac{1}{2}}) + \frac{1}{2}C_s'(\mathcal{J}_5 - \mathcal{J}_6) \\ \mathcal{J}_3 = h_f^2 a^{-2}[C_n'(\mathcal{J}_1^{\frac{1}{2}} - D^{\frac{1}{2}}) \\ \qquad + a^{-2}(C_n' a^2 (C_n' - C_s')\kappa_f^2)(D^{\frac{1}{2}} - \frac{1}{2}D^{\frac{1}{2}} - \mathcal{J}_1^{\frac{1}{2}} - \frac{1}{2}\mathcal{J}_1^{\frac{1}{2}})] \\ \mathcal{J}_4 = (C_n' - C_s') h_f \kappa_f a^{-2}(D^{\frac{1}{2}} - \mathcal{J}_1^{\frac{1}{2}}) \\ \mathcal{J}_5 = \ln \dfrac{\mathcal{J}_1^{\frac{1}{2}} - 1}{\mathcal{J}_1^{\frac{1}{2}} + 1} \\ \mathcal{J}_6 = \ln \dfrac{D^{\frac{1}{2}} - 1}{D^{\frac{1}{2}} + 1} \end{cases}$	(38)

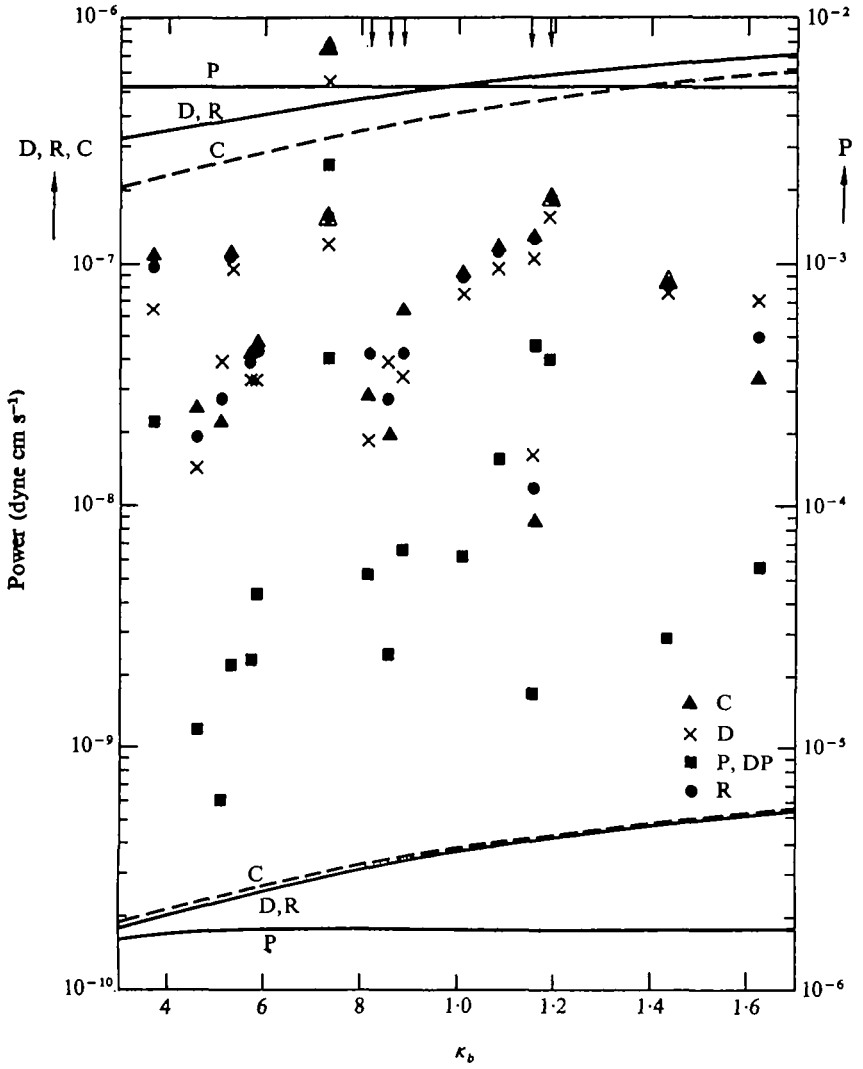

Fig. 8. Power dissipation by swimming Spirilla as a function of body helix pitch. Model symbols shortened as in Fig. 6. The bundle parameters used to generate the 'extrema' model curves and the data points were drawn from within the ranges listed in Table 1. The ordinate on the left is scaled for all the non-parabolic models, and the one on the right for the parabolic models. The arrows at the upper abscissa indicate power values based upon the spin ratios $\Omega/\omega = 0{\cdot}288$.

for the DH model

$$P_{\mathrm{DH}} = P_b + P_d \tag{41}$$

and for the CWW model

$$P_{\mathrm{CWW}} = P_b + P_c (\text{see CWW}). \tag{42}$$

Illustrative 'extrema' curves generated by (39–42) as functions of κ_b are presented in Fig. 8. All parameters were manipulated within the ranges delineated in Table 3. The dynamic variables U, Ω and ω are represented by their maximum measured values in the upper plots and small non-zero values in the lower plots. Specific values of these

Table 8. *Central tendencies of calculated power expenditures by swimming* Spirillum *for four bundle geometry models*

(Values are presented for flagellar bundles P_f, helical body P_b and the entire swimming organism P_{DH}, P_{PB}, P_{RH} and P_{CWW}. Sample sizes N were 18 for all medians. All variances are sample standard deviations which were reduced to values less than the listed averages by discarding the more deviant sample values. Accordingly, the N values refer to the sizes of the samples used to compute the mean values only.)

	Median	Average	N
P_{DH}*	6·46	6·46 ± 4·13	17
P_f*	0·63	0·99 ± 0·75	16
P_{PB}†	5·38	4·40 ± 3·88	13
P_f†	5·38	9·43 ± 9·00	15
P_{RH}*	6·70	7·45 ± 5·12	17
P_f*	1·70	2·24 ± 1·34	17
P_{CWW}*	7·45	7·54 ± 5·35	17
P_f*	2·00	2·34 ± 1·52	17
P_b*	4·07	5·20 ± 4·31	17

* In 10^{-9} dyne cm s^{-1}. † In 10^{-5} dyne cm s^{-1}.

quantities are given in the figure legend. The abscissa to the left in the figure covers the range of values for the RH, DH and CWW models and the one on the right the PB model values which are the same as for the DHPB model when $m = 1$. These results indicate another reason for nature to reject the PB bundle geometry, which is that it is wasteful, as it requires the organism to dissipate swimming energy three orders of magnitude faster than do the other three bundle geometries. The one organism whose data points exceed all the model plots is the one with the hard-to-explain large U. It is possible that the DH model plot could have been adjusted to contain the data plot by inserting a value of $g < 0$ but no observations supported such an adjustment and we have defined $g > 0$. The results illustrated in Fig. 8, then, do support the acceptance of the two helical bundle models. These results are further summarized in Table 8. Here, the central tendency of the values for power dissipation from Fig. 8 are expressed in both median and mean form because the medians could be obtained for all 18 Spirilla while mean values which were greater than their standard deviations were only possible when some members of the sample were ignored. (An examination of Fig. 8 will indicate that the power values for the 6 Spirilla for which $\Omega/\omega = 0{\cdot}288$ clustered around the mean. Accordingly, their exclusion from the mean calculations would have little effect on the mean but their inclusion kept the standard deviations small; so they were included.)

There remains now the task of showing that the power available for *Spirillum* propulsion is sufficient for the hydrodynamic demands of a beating helical bundle. To be sure, the energy generating process for motility is oxidative phosphorylation, but unlike the case for eukaryote motility, ATP is not the energy source (Larsen *et al.* 1974). Unfortunately, the nature of the true energy source is still unknown beyond its appellation 'the intermediate form of energy for oxidative phosphorylation' (Larsen *et al.* 1974). It would be instructive, accordingly, to evaluate the swimming energetics and construct a flagellar motor model based upon an ATP-energized motility. Then, when the necessary information about the true energy sources becomes available, the same procedure may be used to update the model.

Table 9. *A comparison of power dissipation by body and flagellar bundle of* Spirillum *with a representative eukaryote*

	m	f	P_b*	P†	P_b/P	$U/n_b\Lambda$
Spirillum	1	36·8	9·02	0·935–1·02	0·886–0·964	2·19
	2	36·8	9·02	0·968–1·14	0·795–0·931	2·19
	1	49·0	10·91	1·16–1·33	0·820–0·940	3·09
	2	49·0	10·91	1·23–1·56	0·699–0·887	3·09
Ciona sperm‡	1	35	2·27–9·08	4·77–5·45	0·05–0·20	49·5

* In 10^{-6} dyne cm s^{-1}. † In 10^{-7} dyne cm s^{-1}.

‡ These data are calculated from Brokaw (1975, 1965). $n_b\Lambda$ represents the material body length.

The energy metabolism of *Spirillum* is not as well known as that of *E. coli*, another bacterium associated with sewage, but it shall be assumed here that their common environment has selected for a similar physiology. The ultimate generator of energy in a model cell is ATP and, accordingly, the availability of ATP for propulsion determines the energy available to flagellar bundles.

Utilizing the energy data from *E. coli* supplied by Lehninger (1971) one can calculate the total power capacity of a Spirillum cell as $1{\cdot}38 \times 10^{-3}$ dyne cm s^{-1}. Thermodynamic efficiency ϵ can then be used to estimate the portion of total power capacity needed for the work in question. Wilkie (1974) defines $\epsilon = \dot{W}/\Delta\dot{G}$, where $\dot{W}$ is the rate of working and $\Delta\dot{G}$ which is the rate of change of Gibbs' free energy that generates $\dot{W}$ for vertebrate voluntary muscle is about 0·66. The corresponding ϵ for insect fibrillar muscle which exhibits high frequency contractions is about 0·32. As indicated in Table 8 the rate at which biochemical energy must be supplied for *Spirillum* to perform its work against external viscous resistance is about 5×10^{-8} dyne cm s^{-1} which means the $\Delta\dot{G}$ must lie between $6{\cdot}65 \times 10^{-5}$ and $1{\cdot}56 \times 10^{-7}$ dyne cm s^{-1}. If we can assume that $\Delta\dot{G}$ is equivalent to 'power capacity' then the work performed against external viscous resistance requires only a small fraction of the total power capacity of the organism.

With these power data in hand we can return to the question of the internal dynamics of the bacterial flagellum. The purpose here is not to explore the internal resistance problem, which as noted previously, is beyond the scope of the present analysis – an investigation similar to that conducted by Schneider & Doetsch (1974), in which the effects of viscosity on flagellar bundle beat *per se* are used to indicate the magnitude of internal resistance, will be necessary – but to show how power expenditure data may be used to test the feasibility of flagellar contraction models. For the sake of this exercise we shall assume (1) that the power dissipated by internal resistance is negligible and (2) that the work performed at a contraction unit – an attachment–detachment (A–D) cycle – is the same in both vertebrate striated muscle and a prokaryote flagellum. This assumption is invalidated by the work of Larsen *et al.* (1974) and there is no longer a compelling reason for retaining any component of the striated muscle model in constructing a prokaryote contraction model. But since there are no available values for biochemical energy consumed by prokaryote motility, the striated muscle values will have to suffice.

The Berg & Anderson (1973) model considers a rotating shaft flagellum surrounded by an M ring of perimeter $7{\cdot}07 \times 10^{-6}$ cm. The flagellum rotates at 50 Hz and is driven by 3 A–D sites on the M ring each 8×10^{-7} cm in length. Each A–D cycle's frequency is,

then, $(7{\cdot}07 \times 10^{-6}/8 \times 10^{-7}) \times 50 = 442$ Hz. If each A–D site generates a force of $3{\cdot}7 \times 10^{-7}$ dynes then the total power generated by all three A–D sites, which is to say the flagellum, is $3{\cdot}7 \times 10^{-7}$ dyne $\times\, 8 \times 10^{-7}$ cm $\times\, 3 \times 442$ Hz $= 3{\cdot}92 \times 10^{-10}$ dyne cm s^{-1}. This value agrees with the estimate for flagellum power dissipation of 4×10^{-10} dyne cm s^{-1} by Coakley & Holwill (1972). Unfortunately, the latter value is not a useful measure for determining the biochemical energy spent to overcome external resistance because it does not represent the total fraction of externally dissipated power supplied to each flagellum. This fraction must include power dissipated by both the flagellum and the body because the motion of the flagellar bundle used to calculate its hydrodynamic power dissipation is a consequence of both the ΔG supplied and the forces and torques exerted by the fluid on the entire organism. In eukaryote spermatozoa which exhibit a planar flagellar beat, the power fraction spent by the body is 5–20 % of the total for the organism (Brokaw, 1975). Although this fraction is significant, it is not as great as the body fraction for *Spirillum* as indicated in Table 8. Indeed, the average for all specimens in the present study is $61{\cdot}8 \pm 27{\cdot}2$ % for the RH and $72{\cdot}5 \pm 27{\cdot}2$ % for the DH model.

To better illustrate the utility of using the total organism power expenditure for calculations of biochemical energy need as well as for construction of a rotating shaft bacterial flagellum model, we consider a specimen whose bundle frequency is similar to the example from Coakley & Holwill (1972). For this specimen we have $f = 49$ Hz, $m = 2$, $\kappa_b = 0{\cdot}738$, $U/c_b = 0{\cdot}640$, $\Omega/\omega = 0{\cdot}266$ and total power dissipated $P = 5(P_{RH} + P_{DH}) = 1{\cdot}4 \times 10^{-7}$ dyne cm s^{-1}. If we reduce m to 1 then we have $P = 1{\cdot}24 \times 10^{-7}$ dyne cm s^{-1} and if we assume each flagellum receives an equal amount of ΔG and, as they assumed, that there are 200 flagella per bundle, then the externally dissipated power fraction received by each flagellum is $6{\cdot}22 \times 10^{-10}$ dyne cm s^{-1}. If we follow the logic used for the Berg & Anderson (1973) model, then we would have to postulate 5 A–D cycles or crossbridges which would give a power dissipation value of $6{\cdot}54 \times 10^{-10}$ dyne cm s^{-1} per flagellum (including $\frac{1}{200}$ of body).

Finally, the dynamics of *Spirillum* swimming can serve as an example of how natural selection may lead to optimization of a biological function but does not require high efficiency. Chwang & Wu (1971) noted that the hydromechanical efficiency (Power dissipated by flagella/Power dissipated by entire organism) is maximized if a uniflagellated organism with a spherical body thickness-to-flagellum thickness ratio greater than 10 swam with a rotational beat and if one with ratio less than 6 swam with a planar beat. If we ignored the non-sperical shape of *Spirillum* and calculated the body-to-bundle ratio from the b_b and b_f values in Table 3, we would obtain a ration of 5–6 which suggests that this bacterium is grossly inefficient. If, however, we drew a prolate spheroid around the average *Spirilum* ($n_b \lambda_b$ = major axis of spheroid, h_b = minor axis) and used its equivalent sphere radius in place of b_b we would obtain a body-to-bundle ratio of $3{\cdot}8 : 0{\cdot}14 = 28$. The true ratio undoubtedly lies between the values given, but is surely > 10 so it agrees quite well with the rotational resistive theory prediction. In contrast the spermatozoa of the tunicate *Ciona* has a body-to-tail ratio of less than 6 and it swims with a planar beat (although it has been known to rotate (Brokaw, 1975)). The predictable consequences of this diversity are summarized in Table 9. The amount of power dissipated by the Spirillum body is so large as compared to the flagellar bundle that hydromechanical efficiency – in this case $1{\cdot}0 - P_b/P$ – is quite small as

shown in Table 9. This state of affairs is reflected in the relative motion of the two cells (the last column). The more efficient spermatozoan is over 15 times faster than the Spirillum. Yet, no one could claim that the prokaryote is any the less successful for this inefficiency.

Meanings of symbols

b_b material radius of rigid body
b_f material radius of flagellar bundle
C conical bundle beat model of CWW
c_b wave propagation velocity of helical body
c_f wave propagation velocity of helical flagellar bundle
C_m viscous coefficient of moment of force tangent to body
C'_m viscous coefficient of moment of force tangent to bundle
C_n viscous coefficient of force normal to body
C'_n viscous coefficient of force normal to bundle
C_s viscous coefficient of force tangent to body
C'_s viscous coefficient of force tangent to bundle
DHPB damped helix and/or parabola bundle beat model
f_b rotation frequency of body
F_b force on body
F_d force on damped helical bundle
f_f beat frequency of bundle
F_p force on parabolic bundle
F_r force on rigid helical bundle
g damping coefficient
h_b amplitude of body helix
hf amplitude of bundle helix or distance of bundle tip from cone or parabola axis
k_b body wave parameter; $2\pi\lambda_b^{-1}$
k_f bundle wave parameter; $2\pi\lambda_f^{-1}$
l length of unbent bundle
L material body length
m number of flagellar bundles
n_b number of body helical waves
n_f number of bundle helical waves
P total power dissipated; also parabolic bundle model
P_b power dissipated by swimming body
P_d power dissipated by swimming damped helical bundle
P_{DH} power dissipated by organism with damped helical bundle
P_{DHPB} power dissipated by organism with damped helical and/or parabolic bundle
P_f power dissipated by bundle
P_r power dissipated by rigid helical bundle
P_{RH} power dissipated by organism with rigid helical bundle
r body radius
r_b position vector for body
r_d position vector for damped helical bundle beat
RH rigid helical bundle beat model
r_p position vector for parabolic bundle beat

r_r position vector for rigid helical bundle beat
U translational velocity of organism
U volume of body
α average angle formed by bundle geometric axis with x axis
β_b pitch angle of body helix; $\tan^{-1}\kappa_b$
β_f pitch angle of bundle helix; $\tan^{-1}\kappa_f$
γ parabolic coefficient
η hydromechanical efficiency
θ $k_f x + \omega t$
Θ $k_b x - \Omega t$
κ_b $\tan \beta_b$; $k_b n_b$
κ_f $\tan \beta_f$; $k_f h_f$
λ_b wavelength of body helix
λ_f wavelength of bundle helix
Λ arc length
ϕ ωt
ω apparent angular velocity of rotation of flagellar bundle
ω_i whip-torque spin or induced angular velocity of rotation of flagellar bundle
Ω counter-torque spin or apparent body spin

This work was supported by National Science Foundation Grants ENG 74–23008 AO1 and AEN 72–03587 AO1. We should like to thank Dr Charles J. Brokaw for his many useful conversations about this work.

REFERENCES

ABRAM, D. (1969). Basal structures and attachment of the polar flagella of *Spirillum serpens*. *Bact. Proc.* **69**, 29.

BERG, H. & ANDERSON, R. A. (1973). Bacteria swim by rotating their flagellar filaments. *Nature, Lond.* **245**, 380–2.

BROKAW, C. J. (1965). Non-sinusoidal bending waves of sperm flagella. *J. exp. Biol.* **43**, 155–69.

BROKAW, C. J. (1975). Spermatozoan motility: a biophysical survey. *Biol. J. Linn. Soc.* **7** (Suppl. 1), 423–39.

CALLADINE, C. R. (1975). Construction of bacterial flagella. *Nature, Lond.* **255**, 121–4.

CHWANG, A. T. & WU, T. Y. (1971). A note on the helical movement of microorganisms. *Proc. R. Soc. Lond.* B **178**, 327–46.

CHWANG, A. T., WU, T. Y. & WINET, H. (1972). Locomotion of Spirilla. *Biophys. J.* **12**, 1549–61.

COAKLEY, C. J. & HOLWILL, M. E. J. (1972). Propulsion of micro-organisms by three-dimensional flagellar waves. *J. theor. Biol.* **35**, 525–42.

DOETSCH, R. N. (1966). Some speculations accounting for the movement of bacterial flagella. *J. theor. Biol.* **11**, 411–17.

GRAY, J. & HANCOCK, G. J. (1955). The propulsion of sea-urchin spermatozoa. *J. exp. Biol.* **32**, 802–14.

HANCOCK, G. J. (1953). The self-propulsion of microscopic organisms through liquids. *Proc. R. Soc. Lond.* A, **217**, 96–121.

JAROSCH, R. (1972). The participation of rotating fibrils in biological movements. *Acta Protozool.* **11**, 23–38.

KELLER, J. B. (1974). Effect of viscosity on swimming velocity of bacteria. *Proc. Natl. Acad. Sci.* USA, **71**, 3253–4.

KRIEG, N. R., TOMELTY, J. P. & WELLS, J. S. JR. (1967). Inhibition of flagellar coordination in *Spirillum volutans*. *J. Bact.* **94**, 1431–6.

LARSEN, S. H., ADLER, J., GARGUS, J. & HOGG, R. W. (1974). Chemo-mechanical coupling without ATP: the source of energy for motility and chemotaxis in bacteria. *Proc. natn. Acad. Sci. U.S.A.* **71**, 1239–43.

LEHNINGER, A. L. (1971). *Bioenergetics* (ed. W. A. Benjamin), 245 pp. Menlo Park.
LIGHTHILL, M. J. (1975). Flagellar hydrodynamics. *The John von Neumann Lecture, S.I.A.M.*
METZNER, P. (1921). Die Bewegung und Rergbeantwortung der Bipolar begir Belten Spirillea. *Jahr. Wiss. Bot.* **59**, 325–412.
MUSSILL, M. & JAROSCH, R. (1972). Bacterial flagella rotate and do not contract. *Protoplasma* **75**, 465–9.
SCHNEIDER, W. R. & DOETSCH, R. N. (1974). Effect of viscosity on bacterial motility. *J. Bact.* **117**, 696–701.
SMITH, R. W. & KOFFLER, H. (1971). Bacterial flagella. *Adv. Microb. Physiol.* **6**, 219–340.
STRENGTH, W. J. & KRIEG, N. R. (1971). Flagellar activity in an aquatic bacterium. *Can. J. Microbiol.* **17**, 1133–7.
WILKIE, D. R. (1974). The efficiency of muscular contraction. *J. Mechanochem. Cell Mot.* **2**, 257–68.
WILLIAMS, M. A. & CHAPMAN, G. B. (1961). Electron microscopy of flagellation in species of Spirillum. *J. Bact.* **81**, 195–203.

APPENDIX

Mathematical analysis

Element of force

According to the resistive theory of Gray & Hancock (1955) the force generated by an element ds of a swimming wave is the vector sum of its tangential and normal components

$$d\mathbf{F} = d\mathbf{F}_n + d\mathbf{F}_s, \tag{A 1}$$

where

$$d\mathbf{F}_n = -C_n \mathbf{v}_n\, ds \quad \text{and} \quad dF_s = -C_s \mathbf{v}_s\, ds \tag{A 2}$$

and C_n and C_s are defined by Lighthill (1975) as

$$C_n = \frac{4\pi\mu}{\ln\left(\frac{0{\cdot}09\Lambda}{b}\right)} \quad \text{and} \quad C_s = \frac{2\pi\mu}{\ln\left(\frac{0{\cdot}09\Lambda}{b}\right) - \frac{1}{2}}, \tag{A 3}$$

where Λ is the wave arc length, b the element thickness and μ the viscosity in poise.

Keller (unpublished) has recently facilitated the application of this analysis to arbitrary swimming geometries by developing a parametric version of the Gray & Hancock formulation. By converting the velocity vectors to the following form

$$v_n = \mathbf{v}.\mathbf{e}_n \quad \text{and} \quad v_s = \mathbf{v}.\mathbf{e}_s, \tag{A 4}$$

where the $\mathbf{e}$ vectors are unit vectors normal and tangent to ds and in the same plane as

$$\mathbf{v} = \mathbf{v}(u,t) = v_n\mathbf{e}_n + v_s\mathbf{e}_s = \dot{x}\mathbf{i} + \dot{y}\mathbf{j} + \dot{z}\mathbf{k} = \dot{\mathbf{r}}(u,t). \tag{A 5}$$

Here u is the parameter which varies with the geometry of the problem and the dot above $\mathbf{r}$, x, y and z indicate differentiation with respect to time t. Substituting (A 2), (A 4) and (A 5) into (A 1) gives

$$d\mathbf{F} = -C_n(\mathbf{v}.\mathbf{e}_n)\mathbf{e}_n\, ds - C_s(\mathbf{v}.\mathbf{e}_s)\mathbf{e}_n\, ds. \tag{A 6}$$

From vector calculus we use

$$ds = (x'^2 + y'^2 + z'^2)^{\frac{1}{2}}\, du$$

and

$$\mathbf{e}_s(u,t) = \frac{x'\mathbf{i} + y'\mathbf{j} + z'\mathbf{k}}{(x'^2+y'^2+z'^2)^{\frac{1}{2}}},$$

where the primes indicate differentiation with respect to u, to obtain the following

$$d\mathbf{F} = dF_x\,\mathbf{i} + dF_y\,\mathbf{j} + dF_z\,\mathbf{k},$$

where

$$dF_x\mathbf{i} = [-C_n\dot{x}(x'^2+y'^2+z'^2)^{\frac{1}{2}} + (C_n-C_s)x'(x'^2+y'^2+z'^2)^{-\frac{1}{2}}(x'\dot{x}+y'\dot{y}+z'\dot{z})]\,du\,\mathbf{i}$$
$$dF_y\mathbf{j} = [-C_n\dot{y}(x'^2+y'^2+z'^2)^{\frac{1}{2}} + (C_n-C_s)y'(x'^2+y'^2+z'^2)^{-\frac{1}{2}}(x'\dot{x}+y'\dot{y}+z'\dot{z})]\,du\,\mathbf{j}$$
$$dF_z\mathbf{k} = [-C_n\dot{z}(x'^2+y'^2+z'^2)^{\frac{1}{2}} + (C_n-C_s)z'(x'^2+y'^2+z'^2)^{-\frac{1}{2}}(x'\dot{x}+y'\dot{y}+z'\dot{z})]\,du\,\mathbf{k} \tag{A 7}$$

of which we utilize only the dF_x term to represent the element of force of interest.

Element of torque

If the swimming wave rotates then the angular momentum must also be balanced for quasi-steady motion and according to the rotational resistive theory of Chwang Wu (1971) the moment of force on an element of the wave is

$$d\mathbf{M} = d\mathbf{M}_\omega + d\mathbf{M}_\Omega \tag{A 8}$$

where

$$d\mathbf{M}_\omega = \mathbf{r}\times d\mathbf{F} \tag{A 9}$$

and

$$d\mathbf{M}_\Omega = -C_m\boldsymbol{\Omega}ds \quad \text{for which} \quad C_m = 4\pi\mu b^2. \tag{A 10}$$

Upon substituting (A 7) in (A 9) and both (A 9) and (A 10) in (A 8) we obtain the full term for the element of torque, the x component of which is

$$dM_x\mathbf{i} = \left[-C_n(\dot{z}y-\dot{y}z)(x'^2+y'^2+z'^2)^{\frac{1}{2}} + (C_n-C_s)\frac{(y'z-z'y)(x'\dot{x}+y'\dot{y}+z'\dot{z})}{(x'^2+y'^2+z'^2)^{\frac{1}{2}}}\right] \times du\,\mathbf{i} - C_m\Omega_x ds. \tag{A 11}$$

The C_m term shall not be explored further because, as shown in the text, it is small enough to be ignored and its analysis requires complications beyond the level of the present work.

Element of power

The rate of energy expenditure or working by the swimming wave against fluid viscous drag in the x direction is calculated in a straightforward manner from

$$dP = -\mathbf{v}.d\mathbf{F}. \tag{A 12}$$

Accordingly, we substitute (A 5) and (A 7) into (A 12) to obtain for the quasi-steady case

$$dP = -[-C_n(\dot{x}^2+\dot{y}^2+\dot{z}^2)(x'^2+y'^2+z'^2)^{\frac{1}{2}} + (C_n-C_s)(x'\dot{x}+y'\dot{y}+z'\dot{z})^2 \times (x'^2+y'^2+z'^2)^{-\frac{1}{2}}]\,du. \tag{A 13}$$